

Supplementary Information

Organic nanoparticles with ultrahigh stimulated emission depletion efficiency for low-power STED nanoscopy

Zhongwei Man,^{‡a} Zheng Lv,^{‡a} Zhenzhen Xu,^{*a} Hongtu Cui,^b Qing Liao,^a Leming Zheng,^{*b} Xue Jin,^c Qihua He,^b and Hongbing Fu^{*a,c}

^a Beijing Key Laboratory for Optical Materials and Photonic Devices, Capital Normal University, Beijing 100048, China.

^b Key Laboratory of Molecular Cardiovascular Sciences of Ministry of Education, the Institute of Cardiovascular Sciences and Institute of Systems Biomedicine, Peking University Health Science Center, Beijing 100191, China.

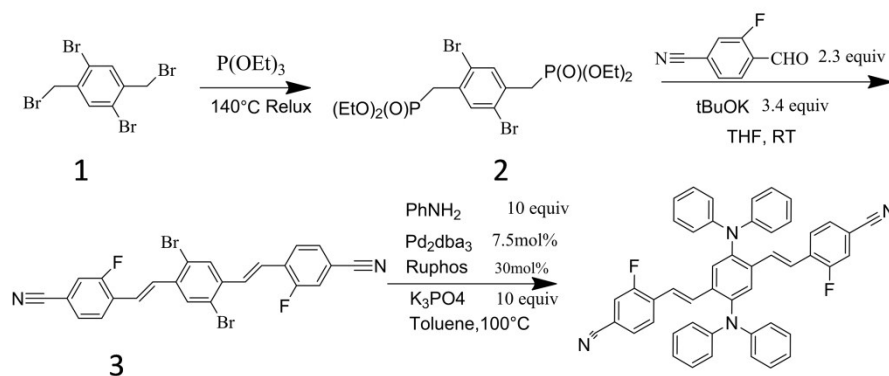
^c Tianjin Key Laboratory of Molecular Optoelectronic Sciences, Institute of Molecular Plus, Tianjin Collaborative Innovation Center of Chemical Science and Engineering, Tianjin University, Tianjin 300072, China.

[‡]These authors contributed equally to this work. Correspondence and requests for materials should be addressed to Z.Z.X. (email: xuzhenzhen@cnu.edu.cn), L.M.Z (zhengl@bjmu.edu.cn) or to H.B.F. (email: hbfu@cnu.edu).

Supplementary Figures:

	Low fluorescence lifetime	High spatial resolution	Low saturation intensity (I_{sat})	High depletion efficiency	photo-bleaching resistance
Qdots	8 ns	78 nm (40 mW)	60 mW	71%	85%
Peversokite QDs	1.51 ns	20.6 nm (22 mW, 7.09 MW cm ⁻²)	0.126 MW cm ⁻²	80%	90%
UCNPs	~ 20 μ s	28 nm (40 mW, 10 MW cm ⁻²)	0.19 MW cm ⁻²	96%	~ 100%
AIE NPs	1.29 ns	30.7 nm (312.5 mW,)	60 mW	75%	~ 96%
ATTO 647N	3.5 ns	163 nm (40 mW, 20 MW cm ⁻²)	20 MW cm ⁻²	80%	70%
DAPF CSONPs	10.6 ns	61 nm (3.56 mW, 0.89 MW cm ⁻²)	0.18 MW cm ⁻²	99%	96%

Table S1. Specific parameters of the reported fluorescent probes-based STED nanoscopy.



Scheme S1. Synthetic route to compound DAPF.

In a 80mL Schlenk tube, the mixture of 2 (0.54 g, 1.0 mmol), *t*-BuOK (0.38 g, 3.4 mmol) in 20 mL THF was controlled in an argon atmosphere. Dissolved 3-fluoro-4-formylbenzonitrile (0.34 g, 2.3 mmol) into 5 mL THF, then the solution was injected into the first mixture. Then, the reaction was kept at room temperature for 1 h before quenching with 20 mL water. All the solvents were filtered and the residue was washed with water (20 mL), EtOH (20 mL), and DCM (20 mL) to obtain the crude product 3. Then the crude 3 was subjected to the following amination without further purification.

In a 10 mL Schlenk tube, the mixture of 3 (0.26 g, 0.5 mmol), Ruphos (69 mg, 0.15 mmol), Pd₂(dba)₃ (34 mg, 0.038mmol), Diphenylamine (0.85 g, 5.0 mmol), K₃PO₄ (1.1 g, 5.0 mmol) were charged with argon. Then the 2 ml toluene was injected into the mixture at room temperature, and the reaction was kept heating at 100°C for 8 h, then cool to room temperature. All the solvents were evaporated. The crude product was obtained by flash chromatography (silica, neutral alumina, eluent: CH₂Cl₂). The

further purification was done by recrystallization in toluene/hexane mixtures, giving the powder (yield=76%).

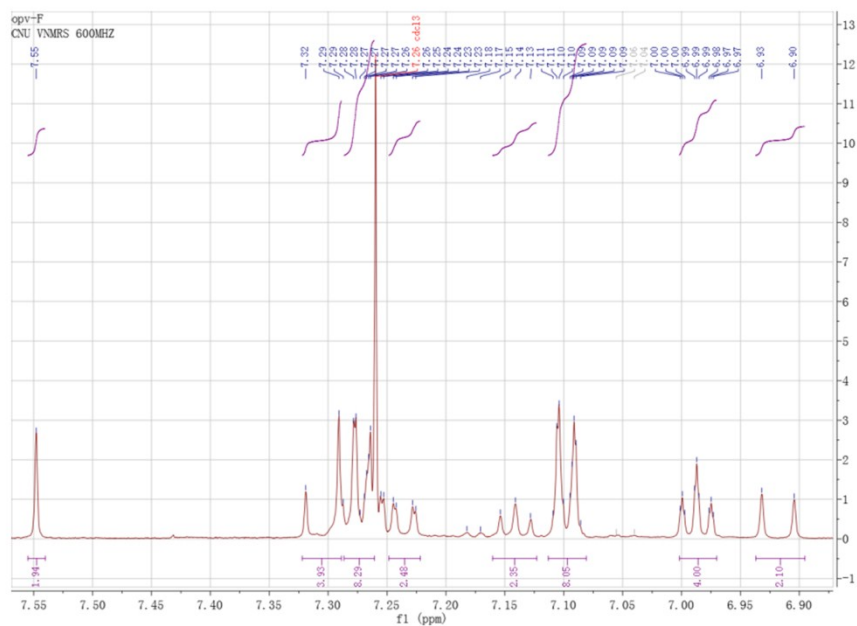


Figure S1. ^1H NMR spectrum of compound DAPF in CDCl_3 at 298 K.

^1H NMR (600 MHz, Chloroform-*d*) δ 7.55 (s, 2H), 7.30 (d, $J = 16.8$ Hz, 4H), 7.29 - 7.26 (m, 8H), 7.24 (dd, $J = 9.9, 1.6$ Hz, 2H), 7.14 (t, $J = 7.7$ Hz, 2H), 7.11 - 7.08 (m, 8H), 6.99 (tt, $J = 7.3, 1.1$ Hz, 4H), 6.92 (d, $J = 16.5$ Hz, 2H).

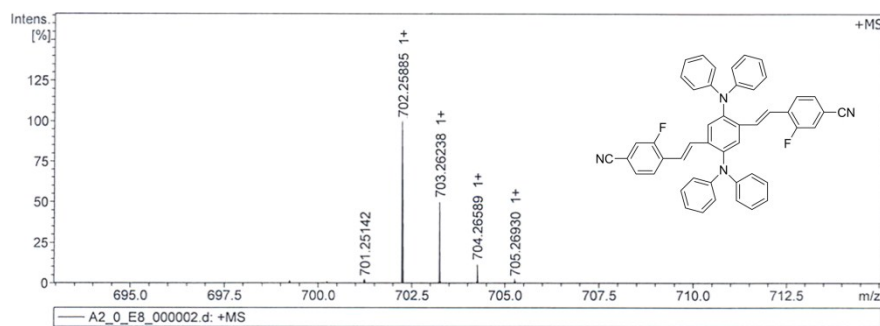


Figure S2. HRMS (ESI) spectrum of compound A1 $m/z = 702$.

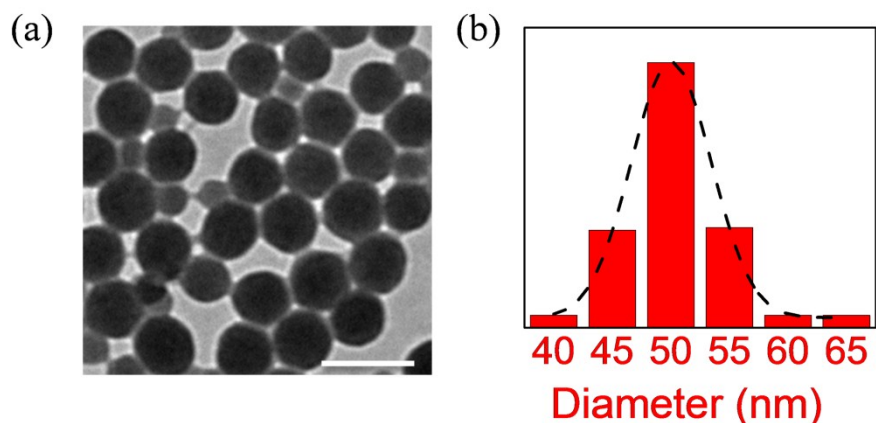


Figure S3. (a) TEM images of DAPF CSONPs. The scale bar is 100 nm. (b) The size distribution of DAPF CSONPs.

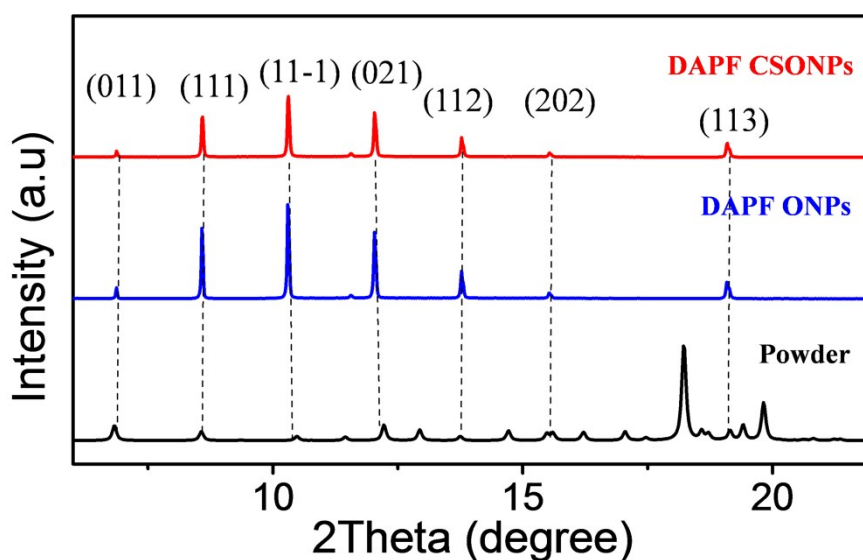


Figure S4. According to Scherrer equation, $\chi = K\lambda/\beta\cos\theta$, where χ is the mean of crystal dimension, K is the shape factor which has a typical value of about 0.9, λ is the X-ray wavelength of 1.54 Å, β is the line broadening at half the maximum intensity in radians, and θ is the Bragg angle. The result shows that the average grain size is about 10-20 nm. As nanoparticles of DAPF CSONPs have an average size of 52 nm, we considered that they are polycrystalline in nature lack of long-range order.

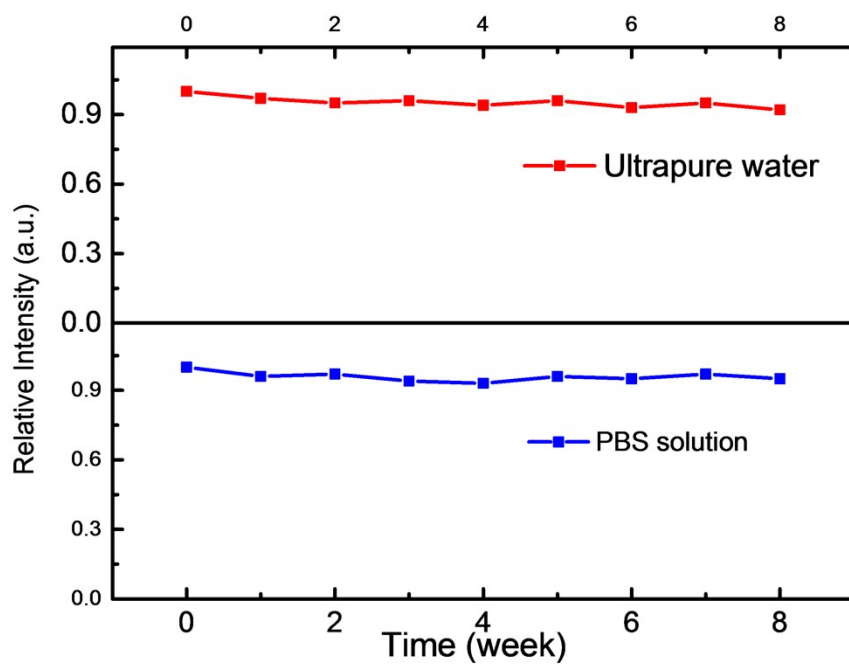


Figure S5. Evolution of the relative fluorescence emission intensity of the DAPF CSONPs upon storage in ultrapure water and PBS solution with time up to 5 weeks.

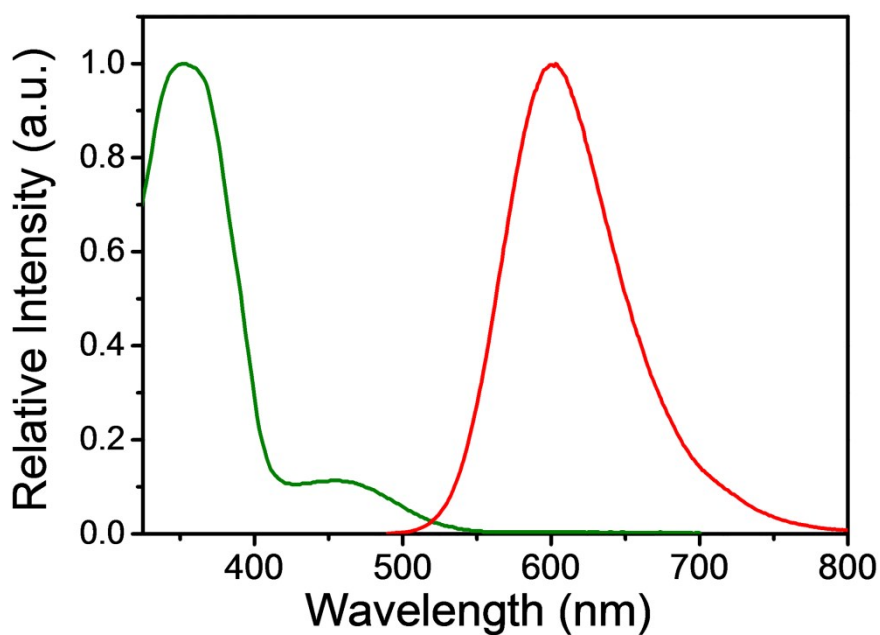


Figure S6. The absorption spectra (green lines) and emission spectra (red lines) of DAPF monomers in THF solution (concentration $C \sim 1.0 \times 10^{-5}$ M).

Compound	$\lambda_{\text{abs}}[\text{nm}]^{[\text{a},\text{b}]}(\epsilon)^{[\text{c}]}$	$\lambda_{\text{em}}[\text{nm}]^{[\text{d}]}(\phi)^{[\text{e}]}$	
		Solution ^[a]	powder Nps ^[f]
DAPF	458(42831)	602(0.57)	605(0.51) 604(0.56)

Table S2. Summary of the synthesized compound DAPF. [a] 1×10^{-5} M in THF. [b] Absorption maximum at the longest wavelength. [c] Molar absorption coefficient [$L \cdot mol^{-1} \cdot cm^{-1}$]. [d] Emission maximum upon photoexcitation at $\lambda=470$ nm. [e] Absolute quantum yield determined with a calibrated integrating sphere system. [f] The nanoparticles of DAPF.

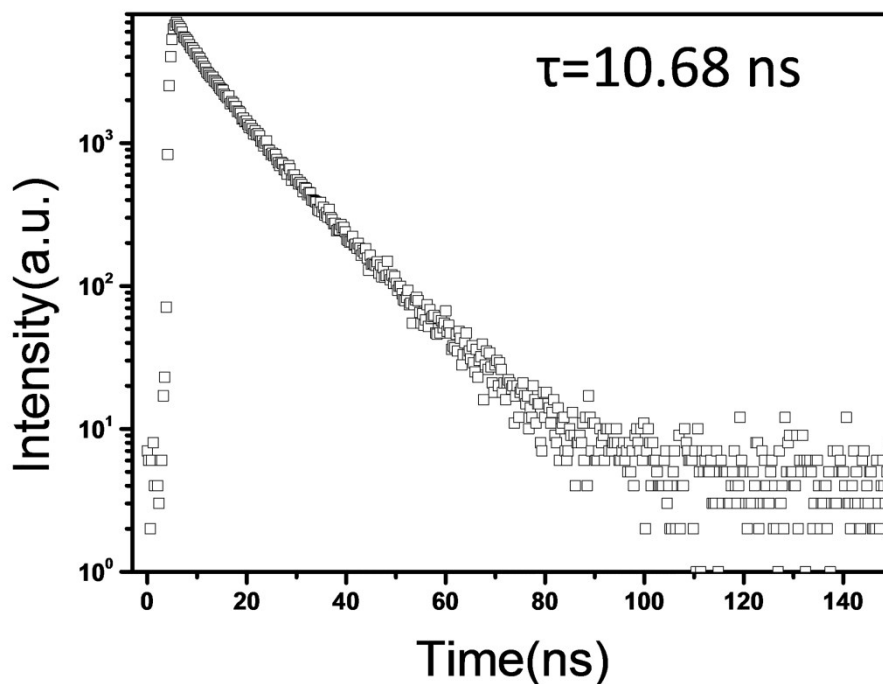


Figure S7. Fluorescence lifetime decay spectra of DAPF CSONPs.

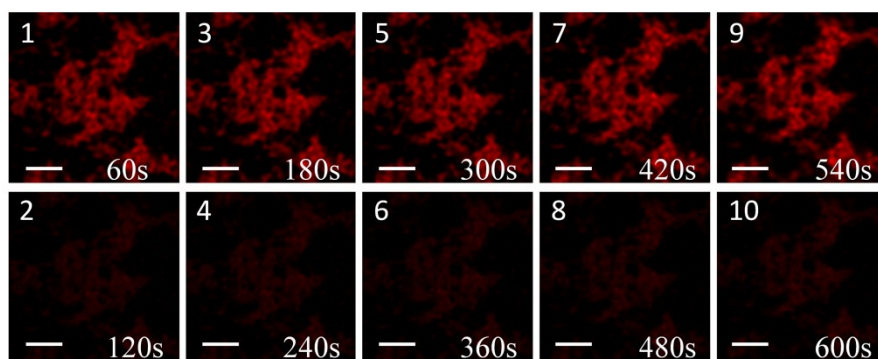


Figure S8. Fluorescence images of DAPF CSONPs irradiated by the 470 nm excitation laser (0.025 KW cm^{-2}) alone (without irradiation of the 660 nm STED laser) (1)(3)(5)(7)(9) and fluorescence images of A2 CSONPs irradiated by the 470 nm excitation laser (0.05 KW cm^{-2}) and 660 nm STED laser (0.49 MW cm^{-2}) (2) (4) (6) (8) (10).

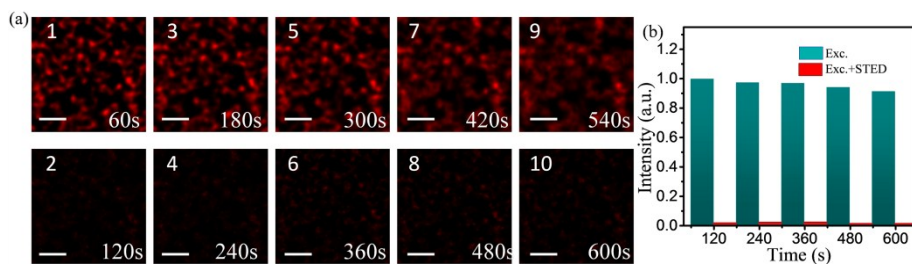


Figure S9. (a) Fluorescence images of DAPF CSONPs irradiated by the 470 nm excitation laser (0.025 KW cm^{-2}) alone (without irradiation of the 660 nm STED laser) (1)(3)(5)(7)(9) and fluorescence images of A2 CSONPs irradiated by the 470 nm excitation laser (0.05 KW cm^{-2}) and 660 nm STED laser (0.89 MW cm^{-2}) (2) (4) (6) (8) (10). (b) Normalized fluorescence intensities of DAPF CSONPs every time point.

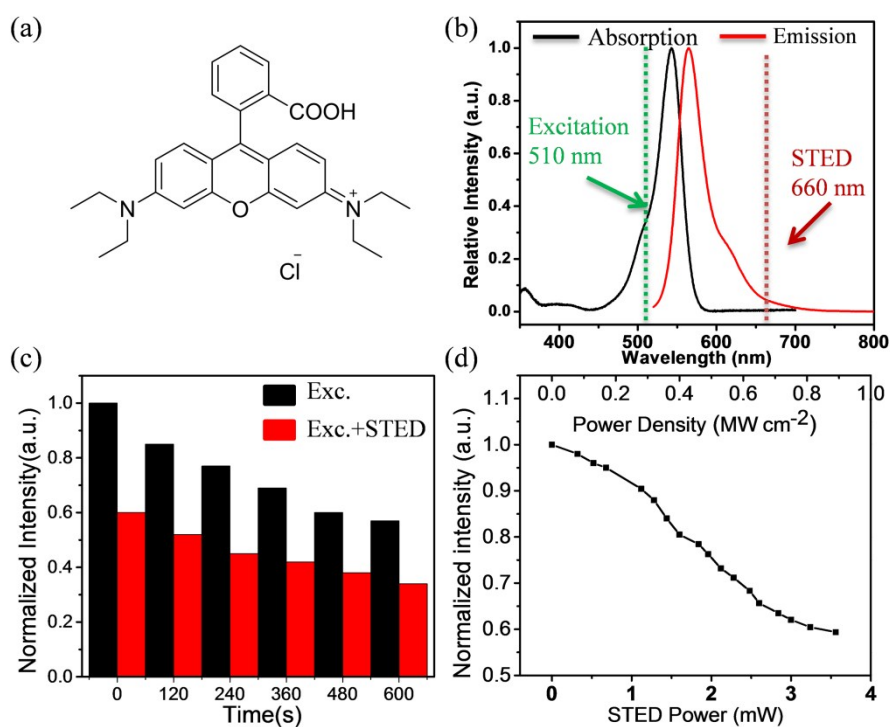


Figure S10. (a) The structure of commercial fluorescent dye Rhodamine B. (b) One photon absorption and fluorescence spectra of Rhodamine B and the selection of the excitation beam and STED beam. (c) Normalized fluorescence intensity of Rhodamine B under the same experiment condition in the above cyclic process. (d) Stimulated emission depletion efficiency of Rhodamine B.

According to the normalization results, the fluorescence intensity of the Rhodamine B film under irradiation of the 470 nm excitation beam (the dark green histogram) was fallen by 40% after 600 s circulation.

$$I_{sat} = \frac{h\nu_{STED}}{\tau * \sigma_{STED}}$$

(Where $h\nu_{STED}$ denotes the STED photo energy, σ_{STED} is the cross-section for stimulated emission, τ is the lifetime of the excited state.)

	h	ν_{STED}	τ	I_{sat}
CSNOPs	$6.62*10^{-34} \text{ J} \cdot \text{s}$	$4.54*10^{14} / \text{s}$	10.68 ns	0.98 MW cm^{-2}
ATTO 647N			3.5ns	20 MW cm^{-2}

Table S3. The photophysical parameters of DAPF CSNOPs and ATTO 647N, respectively.

The calculated stimulated emission cross section corresponding to the above equation and Table S3 are $\sigma_{\text{DAPF CSNOPs}} = 2.87*10^{-17} \text{ cm}^2$, $\sigma_{\text{ATTO 647N}} = 4.29*10^{-18} \text{ cm}^2$, respectively. Therefore, the stimulated emission cross section of DAPF CSNOPs is increased by 6.6 times compared with that of ATTO 647N. This high stimulated emission cross section results in lower saturation intensity of DAPF CSNOPs. The further measurement of the stimulated radiation cross-section is underway.

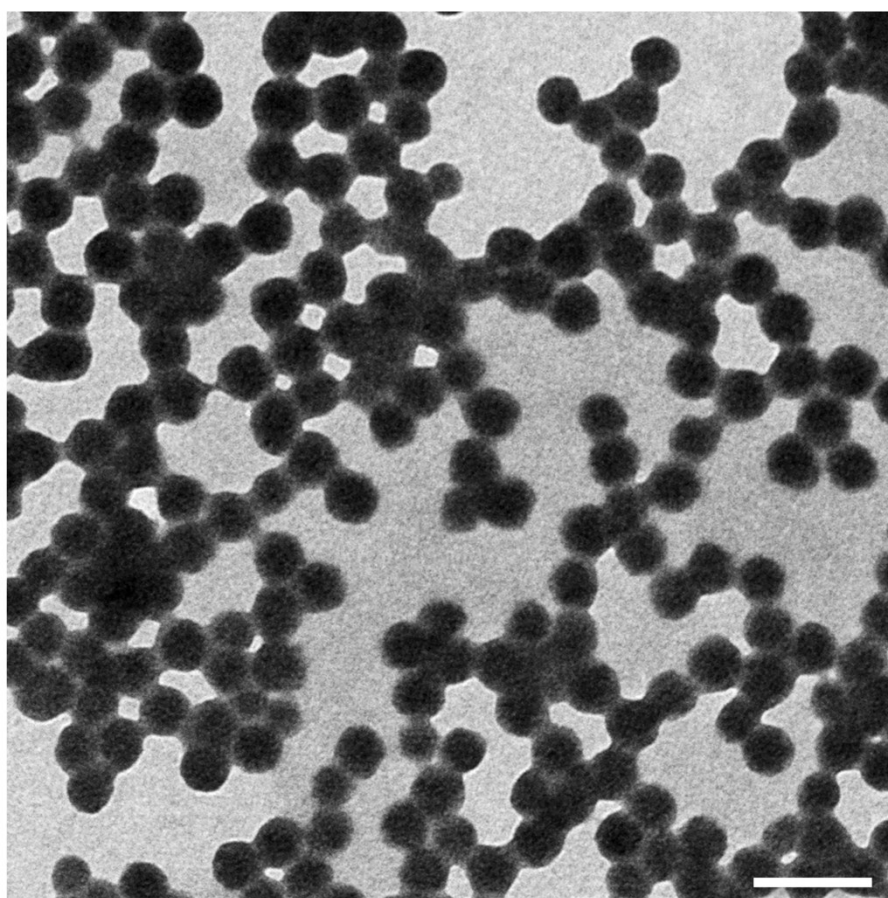


Figure S11. TEM image of 30 nm DAPF CSNOPs. The scale bar is 60 nm. As seen in Fig S11, transmission electron microscope images reveal a spherical

morphology with an average diameter of ~ 26 nm and a silica shell thickness of 3-5 nm.

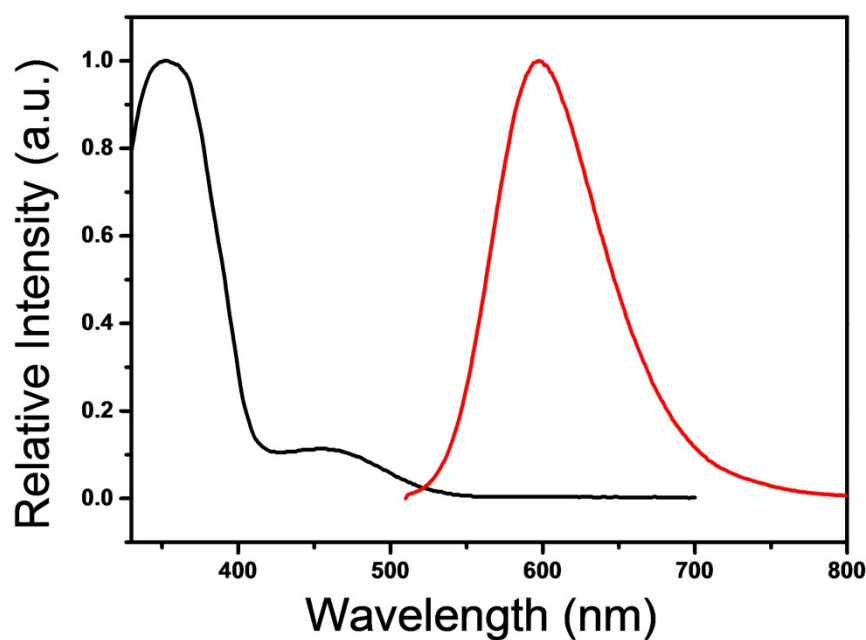


Figure S12. The absorption spectrum (the black line) and the emission spectrum (the red line) of 30 nm DAPF CSONPs.

As shown in Fig S12, the absorption and emission maximum of 26 nm DAPF CSONPs are 352 and 604 nm, respectively, which remain the same as the nanoparticles with size of 50 nm (352 and 604 nm, respectively).

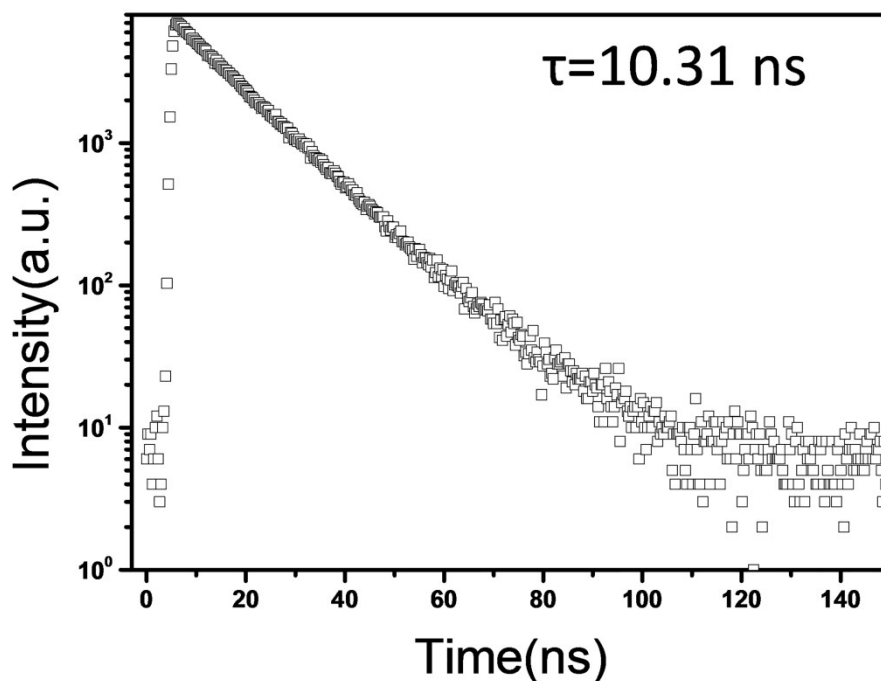


Figure S13. The fluorescence lifetime of 30 nm DAPF CSONPs.

As shown in Fig S13, it can be seen that the fluorescence lifetime of 26 nm DAPF

CSONPs is 10.31 ns, which remain the same as the nanoparticles with size of 50 nm (10.68 ns).

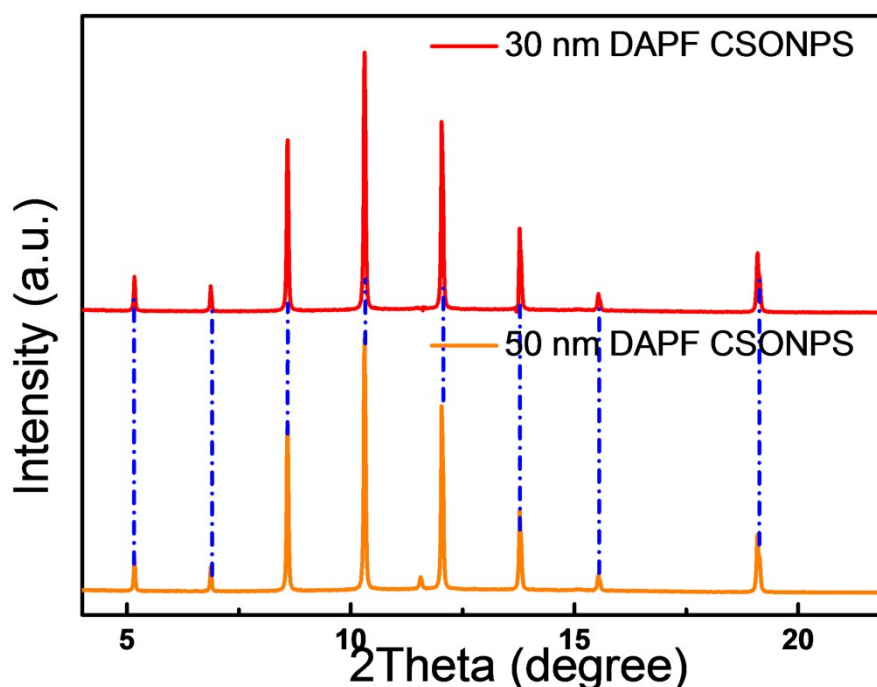


Figure S14. XRD patterns of 30 nm DAPF CSONPs and 50 nm DAPF CSONPs. As shown in Fig S14, the X-ray diffraction pattern of 26 nm DAPF CSONPs agreed well with that of 50 nm DAPF CSONPs, suggesting that the 26 nm DAPF CSONPs adopted the same molecular packing mode as 50 nm DAPF CSONPs.

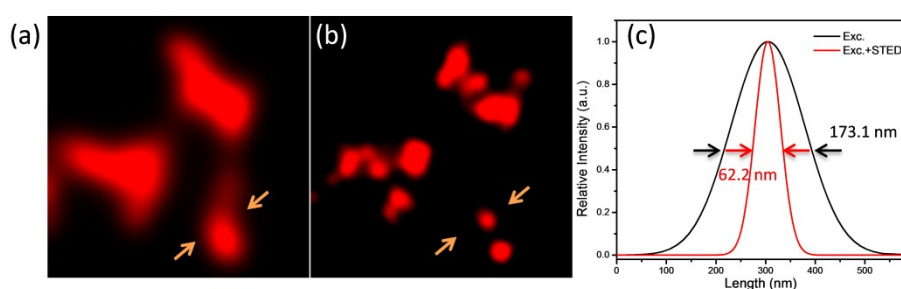


Figure S15. (a) Fluorescence images of 26 nm DAPF CSONPs irradiated by the 470 nm excitation laser beam (0.025 KW cm^{-2}) alone. (b) The corresponding fluorescence images of 26nm DAPF CSONPs irradiated by the 470 nm excitation laser (0.05 KW cm^{-2}) and 660 nm STED laser (0.89 MW cm^{-2}) simultaneously. (c) Normalized fluorescence intensity profiles across the nanoparticle in (a) and (b)

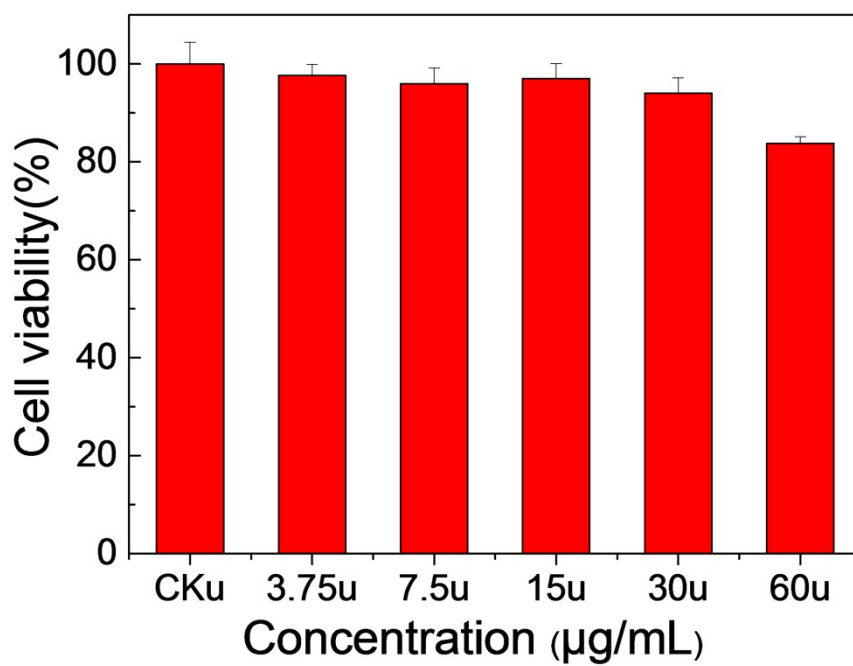


Figure S16. Viability of HeLa cells treated with various concentrations of DAPF CSONPs for 24 hours.

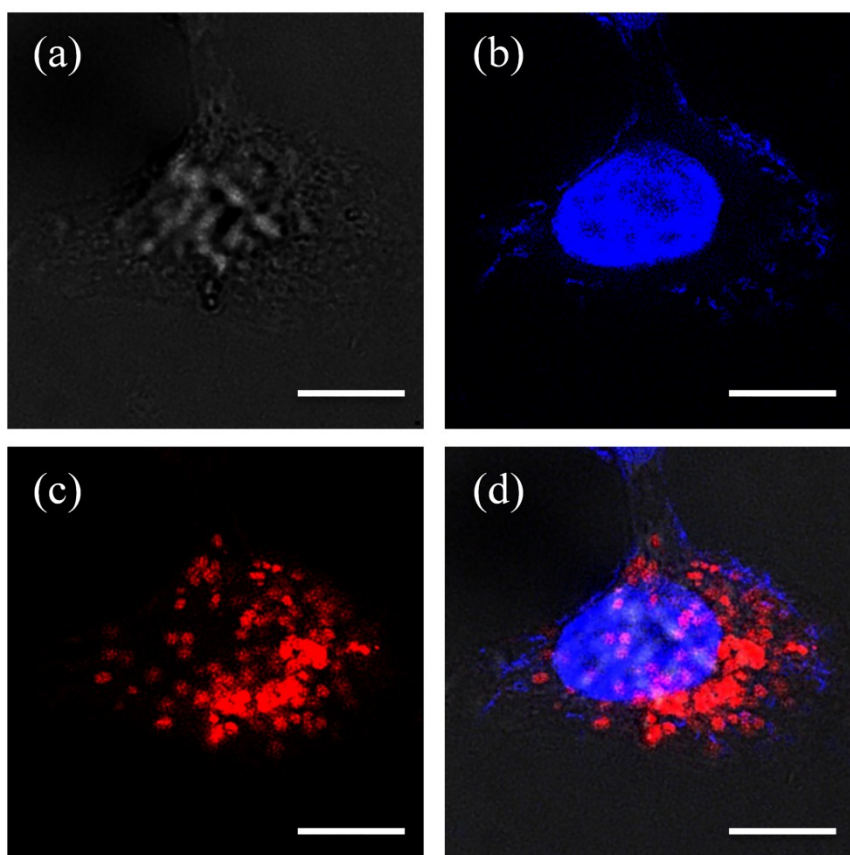


Figure S17. (a) The bright field image of DAPI and DAPF CSONPs co-stained HeLa cell. Confocal images of HeLa cell stained with (b) DAPI and (c) DAPF CSONPs (0.026 mg mL^{-1}) for 0.5 h; and (d) the merged picture of (b) and (c). The scale bar in (a-d) is $8 \mu\text{m}$.

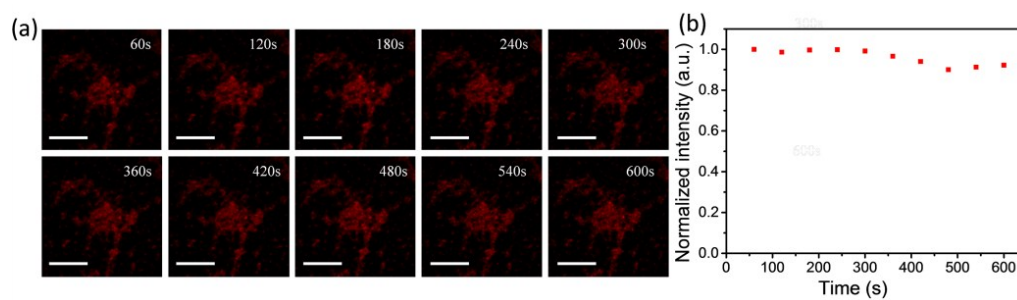


Figure S18. (a) STED nanoscopic images of DAPF CSONPs taken at various time points. The scale bar is $3 \mu\text{m}$. (b) Normalized fluorescence intensity of DAPF CSONPs at various time points, during 600 continuously scanning of the 470 nm excitation beam (0.05 KW cm^{-2}) and the 660 nm STED beam (0.49 MW cm^{-2}).